Summer 2017

Iterative learning control for improved tracking of fluid percussion injury device

Steve Susanibar
New Jersey Institute of Technology

Copyright Warning & Restrictions

The copyright law of the United States (Title 17, United States Code) governs the making of photocopies or other reproductions of copyrighted material.

Under certain conditions specified in the law, libraries and archives are authorized to furnish a photocopy or other reproduction. One of these specified conditions is that the photocopy or reproduction is not to be "used for any purpose other than private study, scholarship, or research." If a, user makes a request for, or later uses, a photocopy or reproduction for purposes in excess of "fair use" that user may be liable for copyright infringement,

This institution reserves the right to refuse to accept a copying order if, in its judgment, fulfillment of the order would involve violation of copyright law.

Please Note: The author retains the copyright while the New Jersey Institute of Technology reserves the right to distribute this thesis or dissertation

Printing note: If you do not wish to print this page, then select "Pages from: first page # to: last page #" on the print dialog screen

ABSTRACT

ITERATIVE LEARNING CONTROL FOR IMPROVED TRACKING OF FLUID PERCUSSION INJURY DEVICE

by
Steve Susanibar

Traumatic brain injury (TBI) afflicts over 10 million people around the world. Injury to the brain can occur from a variety of physical insults and the degree of disability can greatly vary from person to person. It is likely that the wide range of TBI outcomes may be due to the magnitude, direction, and forces of biomechanical insult acting on the head during such TBI events. Lateral Fluid Percussion (FPI) brain injury is one of the most commonly used and well-characterized experimental models of TBI. A Fluid Percussion Injury (FPI) device in the laboratory is used to replicate the injury but does not execute the desired pressure profile. The controller used is a QCI-S3-IG Silver Sterling from Quick Silver Controls. A limitation innate to the controller was a 3-millisecond sampling of the input signal that proved challenging for developing fast, accurate FPI pulses with periods as fast as 18-milliseconds. Iterative Learning Control is implemented which conditions the input signal to the open loop system offline such that the desired pressure profile is attained.

ITERATIVE LEARNING CONTROL FOR IMPROVED TRACKING OF FLUID PERCUSSION INJURY DEVICE

by
Steve Susanibar

A Thesis
Submitted to the Faculty of
New Jersey Institute of Technology
in Partial Fulfillment of the Requirements for the Degree of
Master of Science in Electrical Engineering

Helen and John C. Hartmann Department of
Electrical and Computer Engineering

August 2017

APPROVAL PAGE

ITERATIVE LEARNING CONTROL FOR IMPROVED TRACKING OF FLUID PERCUSSION INJURY DEVICE

Steve Susanibar

Dr. Cong Wang, Thesis Advisor Assistant Professor of Electrical and Computer Engineering, NJIT	Date
Dr. Bryan J. Pfister, Committee Member Professor of Biomedical Engineering, NJIT	Date
Dr. Xuan Liu, Committee Member Assistant Professor of Electrical and Computer Engineering, NJIT	Date

BIOGRAPHICAL SKETCH

Author: Steve Susanibar

Degree: Master of Science

Date: August 2017

Undergraduate and Graduate Education:

- Master of Science in Electrical Engineering,
  New Jersey Institute of Technology, Newark, NJ, 2017

- Bachelor of Science in Applied Physics,
  New Jersey Institute of Technology, Newark, NJ, 2015

Major: Electrical Engineering

I dedicate this work to my parents who have always supported me in all my endeavors.

ACKNOWLEDGMENTS

I would like to express my deepest gratitude to my thesis advisor, Dr. Cong Wang, for his selection of this topic, guidance and support throughout the process of this work.

I would also like to express my utmost appreciation to the committee members of my thesis Dr. Bryan Pfister and Dr. Xuan Liu.

TABLE OF CONTENTS

LIST OF TABLES

Table **Page**

LIST OF FIGURES

CHAPTER 1

INTRODUCTION

1.1 Motivation - Traumatic Brain Injury

Every year, an estimated 1.7 million Americans and 10 million people worldwide sustain a Traumatic Brain Injury (TBI) [1, 6]. TBI is predominant in low to middle-income countries and is correlated with the risk factors and availability of medical treatment in the particular countries. Injury to the brain can occur from a variety of physical insults and the degree of disability can greatly vary from person to person. TBI can occur from a variety of physical insults to the brain from sources such as automobile accidents, sport collisions or blast waves, for example. It is likely that the wide range of TBI outcomes may be due to the magnitude, direction, and forces of the biomechanical insult acting on the head during these insult-driven events.

The severity in terms of brain pathology and behavioral outcomes in the majority of TBI studies is associated with the magnitude of the primary injury. Research has just begun on the contributions that the temporal characteristics of the injury such as rise time (calculated as the pressure rise from 10% to 90 % of the peak representing the rate at which the injury was delivered) and duration of impact have on damage to the brain [4, 5]. In closed-head injuries, where no craniotomy is made, axon damage is believed to be caused by brain deformation in response to insults [7, 8, 13]. Used to deform the brain of rodents to produce both focal and diffuse injury characteristics, lateral fluid percussion injury (FPI) is one of the most commonly used and well-characterized experimental models of TBI].

Potentially one of the biggest contributors to differences in TBI outcome could be the rate at which pressure changes in addition to magnitude of the pressure that deforms the brain [3]. Rate refers to the rise time to peak pressure. Since the brain is viscoelastic, both rate and magnitude of the pressure will affect how the tissue responds mechanically and hence lead to unique pathophysiologies [3]. To illustrate two impacts that differ in magnitude, compare a head impact from a fall versus a blast wave; in this case, the latter is several orders of magnitude higher.

Early head injury physical models discovered injury correlated with rotational acceleration of the head [10]. At the time of writing, there are no animal models directly examining whether the pathophysiological outcome of injury depends on the rate of the delivered injury. This is due to the limitations of the available animal models to adjust for injury magnitude. For instance, FPI and weight drop injury vary either by height adjustment of the pendulum in FPI [12] or by height or mass adjustment of the dropped weight [11]. The miniature pig injury model is the exception to this. In this model, rotational acceleration is adjustable and thus the device rapidly rotates the animal's head over the designated angular profile at predetermined angular accelerations, which correlates with severity of diffuse brain trauma. Unfortunately the model is difficult to duplicate and not widely used.

1.2 Methods of Studying Traumatic Brain Injury

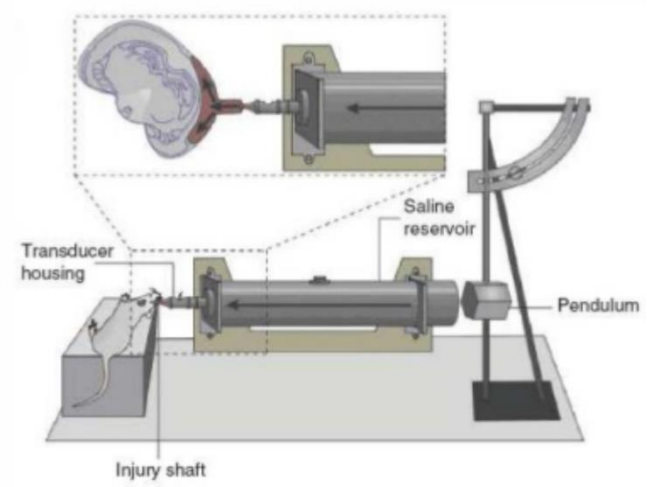

Figure 1.1 Pendulum fluid percussion injury setup consists of a pendulum and saline reservoir.

Source: National Center for Biotechnology Information

In the pendulum fluid percussion injury (PFI) setup a cylindrical tube filled with saline fills the interstitial space above the dura without causing skull fracture to produce a rapid displacement and deformation of brain tissue. Indeed, it has been found suitable for the study of injury pathology, physiology, and pharmacology in a wide range of species, including rats, mice, cats, pigs, rabbits, and dogs and sheep. In this model, the insult is inflicted by application of a fluid pressure pulse to the intact dura through a craniotomy, which is made laterally usually over the left parietal bone; the craniotomy may be in combination with or without a contralateral skull opening. Briefly, the anesthetized animals are placed in a stereotaxic frame and their scalp and temporal muscles reflected. A small craniotomy is made to allow insertion of a plastic cap that is cemented into place. The FPI device consists of a Plexiglas cylindrical reservoir filled with sterile isotonic saline. One

end of the reservoir includes a transducer, which is mounted and connected to a tube that attaches through a plastic fitting to the cap cemented on the animal's skull at the time of surgery. The strike of a pendulum at the opposite end of the cylindrical reservoir generates a pressure pulse that is delivered to the intact dura and instigates deformation of the underlying brain. The severity of injury depends on the pressure pulse.

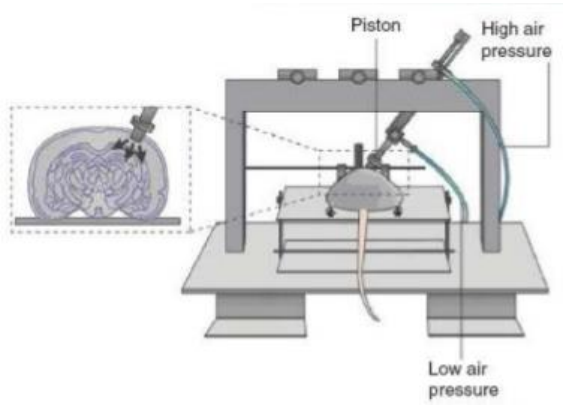

Figure 1.2 Controlled Cortical Impact set up with rigid impactor and cranial cross section view.

Source: National Center for Biotechnology Information

Controlled Cortical Impact (CCI) devices are also used to study TBI. The CCI device, characterized as direct and localized injury, was designed for simulating penetrating injury. In a CCI device, a pneumatic or electromagnetic impact device drives a rigid impactor onto the exposed, intact dura and imitates cortical tissue loss, acute subdural hematoma, axonal injury, concussion, blood-brain barrier dysfunction and even coma. Ferret, rat, and mouse have been primary subjects of study for this type of head trauma. This model allows for better control over mechanical factors, such as velocity of impact and depth of resulting deformation, thus offering potential advantages over the fluid percussion model, especially in biomechanical studies of TBI.

The device used in rodent CCI models consists of a pneumatic cylinder usually with a 4 to 5-cm stroke, which is mounted on a cross bar so that the position of the impactor can be adjusted. The impact velocity used in the majority of studies is between 0.5 and 10 m/s depending on air pressure that drives the impactor. The depth of cortical deformation is controlled by vertical adjustment of the crossbar holding the cylinder and can be varied from between 1 and 3-mm, whereas the duration of the impact (dwell time) can be adjusted between 25 and 250-milliseconds. It has been shown that cerebral hemodynamic responses such as elevated intracranial pressure, decreased blood and cerebral perfusion pressures, histological, and cellular alterations, as well as functional deficits are related to both the depth of deformation and the velocity of the impact. Impacts inflicted at a velocity higher than 4.3 m/s (4.3– 8.0 m/s) and with a depth of cortical deformation from 1.0 mm initiate widespread acute and chronic neuronal injury [15].

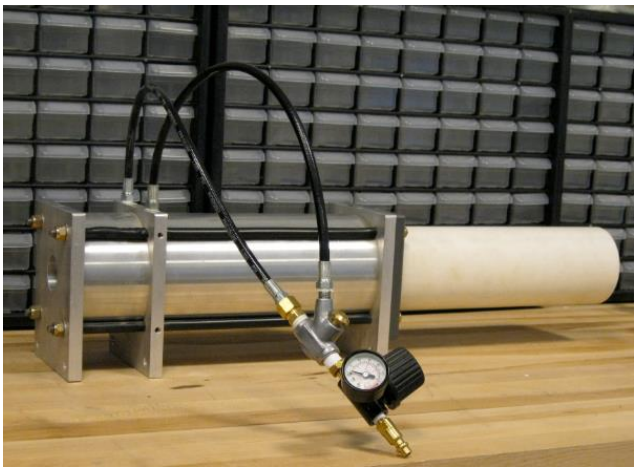

Figure 1.3 Shock tube of length 26 inches comprised of an aluminum exterior with vasiform exposure chamber.

Shock tube proceedings operate in a similar fashion. Shock tubes have shown to produce fast, short duration impacts. A pressure of 25 PSI can be released in under 3-milliseconds utilizing air-gun technology [16]. A transient shock loading will be generated using an unstable pneumatic valve, which releases a pressure wave from pressurized reservoir. The air pressure is user set and determines the peak amplitude of the shock loading. The unstable valve is triggered by an unbalance in air pressure between the two sides of the valve. The shockwave is released into a vasiform exposure chamber where the animal is placed [16].

CHAPTER 2

FLUID PERCUSSION

2.1 Introduction to Fluid Percussion

Fluid percussion injury (FPI) models or simply FPI models is one of the most frequently used direct brain deformation models. It has been found suitable for the study of injury pathology, physiology, and pharmacology in a wide range of species, including rats, mice, cats, pigs, rabbits, and dogs and sheep. In this model, the insult is inflicted by application of a fluid pressure pulse to the intact dura through a craniotomy; the craniotomy may be in combination with or without a contralateral skull opening. As mentioned previously, TBI studies link the magnitude of the primary injury, to severity in terms of brain pathology and behavioral outcomes, in this case the peak pressure in the FPI model.

To produce a controlled fluid percussion, a voice coil actuator can be utilized to generate a precise temporal forcing function under closed loop control with a motion controller rather than applying a pendulum as the concussive force origin. The voice coil coupled to a hydraulic cylinder filled with isotonic water delivers the defined percussion waveform [14].

2.2 Setup

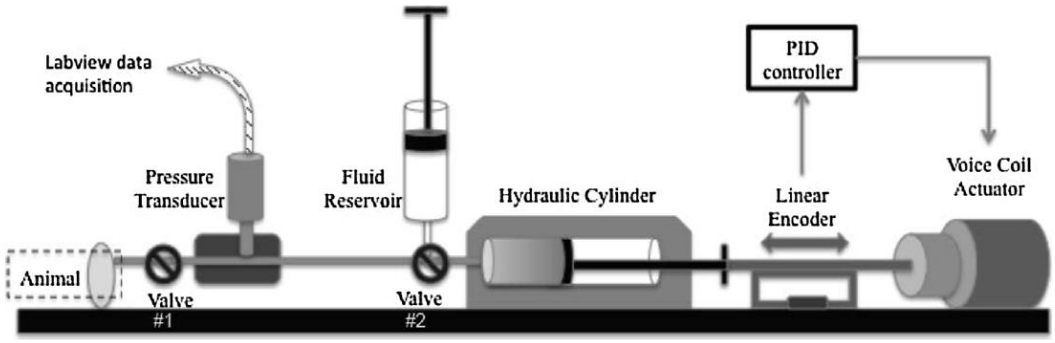

Figure 2.1 The FPI experimental setup with animal included.

A voice coil-driven, actuator fluid percussion injury system controlled by an external computer was developed to precisely control the characteristics of the pressure waveform including rise time and peak pressure. Fluid percussions were generated by moving a rigidly connected hydraulic cylinder with a linear voice coil actuator (LAS28-53-000A, BEI Kimco). Accordingly, the controlled motion of the voice coil and hydraulic cylinder translates into a controlled rise in fluid pressure. The movement of the voice coil actuator is controlled by the QCI-S3-IG Silver Sterling Controller from Quick Silver Controls. A linear optical encoder (TONiC T100x RGSZ) was placed underneath the rod of the linear drive to track the displacement of the plunger rod of the hydraulic cylinder. A flat-faced pressure transducer (px61v0-100gv, Omega-dyne) was mounted at the output of the hydraulic cylinder to measure the applied fluid percussion. LabVIEW from National Instruments collected the fluid percussion, pressure data for exporting into Excel.

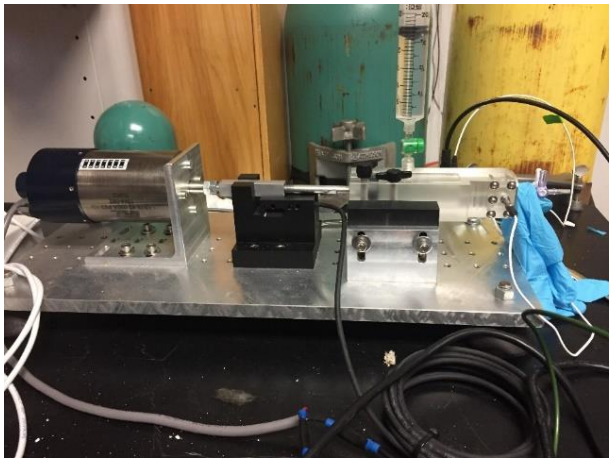

Figure 2.2 The FPI experimental setup with stopper and plastic barrier in replacement of the rodent. From left to right: Voice coil actuator, linear encoder, hydraulic cylinder with reservoir, transducer, and stopper with rubber barrier (as Latex glove in picture).

A green valve showed in the picture seals off the fluid reservoir to the hydraulic cylinder. In place of the animal on the end of the hydraulic is a closed valve in with a latex glove to serve as the simulated rodent tissue. Once the controller relays a set of motion commands to the voice coil, the voice coil drives the piston in the hydraulic cylinder forward and returns back to its original position. Whilst the motion commands are executed, the transducer records the pressure profile and reads them into LabVIEW.

CHAPTER 3

ITERATIVE LEARNING CONTROL

3.1 Introduction to Iterative Learning Control

The premise of Iterative learning control (ILC) is that the performance of a system that executes the same task multiple times can be improved by learning from previous executions (trials or iterations). During a regulation basketball game, a player will attempt many shots from different spots on the court. These players strengthen their shooting technique of scoring a basket by practicing the shot repeatedly. For every shot the basketball player is unsuccessful, he adjusts his technique which may consist of applying more force from his legs, snapping his wrist more quickly or changing his body orientation with respect to the basket. As the player continues to practice, the correct execution is learned and is remembered by his nervous system so that the shooting accuracy is iteratively improved. The converged muscle motion profile is an open-loop control generated through repetition and learning. This type of learned open-loop control strategy is the essence of ILC.

We consider learning controllers for systems that perform the same operation repeatedly and under the same operating conditions. For such systems, non-learning controller yields the same tracking error on each pass. Although the signals from previous iterations are information rich, they are unused by a non-learning controller. The objective of ILC is to improve performance by incorporating error information into the control for subsequent iterations. In doing so, high performance can be achieved with low transient tracking error despite large model uncertainty and repeating disturbances.

ILC differs from other learning-type control strategies such as adaptive control, neural networks, and repetitive control (RC). Adaptive control strategies modify the controller, which is a system, whereas ILC modifies the control input, which is a signal. Additionally, adaptive controllers typically do not take advantage of the information contained in repetitive command signals. Similarly, neural network learning involves the modification of controller parameters rather than a control signal; in this case, large networks of nonlinear neurons are modified. These large networks require extensive training data, and fast convergence may be difficult to guarantee whereas ILC usually converges adequately in just a few iterations [17].

ILC is perhaps most similar to Repetitive Control (RC) except that RC is intended for continuous operation, whereas ILC is intended for discontinuous operation. For example, an ILC application might be to control a robot that performs a task, returns to its home position, and comes to a rest before repeating the task. On the other hand, an RC application might be to control a hard disk drive's read/write head, in which each iteration is a full rotation of the disk and the next iteration immediately follows the current iteration.

Traditionally, the focus of ILC has been on improving the performance of systems that execute a single, repeated operation. This focus includes many practical industrial systems in manufacturing, robotics, and chemical processing, where mass production on an assembly line entails repetition. ILC has been successfully applied industrial tools, wafer stage motion systems, injection-molding machines, aluminum extruders, cold rolling mills, induction motors, chain conveyor systems, camless engine valves, autonomous vehicles, antilock braking, rapid thermal processing, and semibatch chemical reactors. Additionally, ILC designs using discrete-time linearizations of nonlinear systems often yield good results when applied to the nonlinear systems.

3.2 Iterative Learning Control Basics

An intuitive way to understand the basic idea of ILC is using an analogy to Newton's method in numerical analysis. In order to find a solution of the equation $f(x)=0$, an iterative numerical algorithm via Newton's method is

$$x_{j+1} = x_j + L \cdot f(x_j), \tag{3.1}$$

where a good choice for the step size coefficient L is $-(f'(x_k))^{-1}$. Analogously, one can consider the response of a control system

$$y = P(u+d) \tag{3.2}$$

$$e = r - y \tag{3.3}$$

Where P represents the input-output dynamics of the system; $u, d, y, r,$ and e are the plant input, the disturbance, the plant output, the reference signal and the tracking error. The idea is to find a (feedforward) control that gives a zero error. This can be achieved using an iterative control learning law

$$u_{j+1} = u_j + Le_j \tag{3.4}$$

Where L is the learning filter, j is the iteration index.

3.3 Method

Plant inversion methods use models of the inverted plant dynamics as the learning function. The discrete-time plant inversion ILC algorithm is given by:

$$u_{j+1}(k) = u_j(k) + \hat{P}^{-1}(q)e_j(k) \tag{3.5}$$

In this form, the learning function L is chosen to be the inverse of the nominal plant, $\hat{P}$. In this equation k is the time index. Assume that the disturbance and reference are consistent over iterations. As per the learning law, the tracking error evolves as

$$\begin{aligned} e_{j+1} &= r - Pu_{j+1} - Pd \\ &= (r - Pu_{j+1} - Pd) - PLe_j \\ &= (I - PL)e_j \end{aligned} \tag{3.6}$$

As long as the gain of $I - PL$ is below 0 dB, the tracking error will converge to zero over iterations. Sometimes $I - PL$ cannot achieve a gain below 0 dB at all frequencies. In this situation, a Q-filter is required to restraint the learning in certain frequency bands [17]. Thus, the corresponding learning law and the error convergence condition are

$$u_{j+1} = Q(u_j + Le_j) \tag{3.7}$$

$$\|Q(I - PL)\| < 1$$

Another method popular in the literature is the PD ILC which requires tuning of gains to assure proper convergence to the desired signal. The PD ILC form is as follows:

$$u_{j+1} = Q(\mathrm{q})[\mathrm{u}_j(k) + k_p e_j(k+1) + k_d(e_j(k+1) - \mathrm{e}_j(k))], \tag{3.8}$$

Where j is the index of iteration, k is the discrete time variable, $Q(\mathrm{q})$ is the Q-filter, K_p is the gain, K_d is the gain, and e is the error signal.

3.3.1 Plant Inversion

By rewriting the learning algorithm, we see that the plant-inversion learning function is causal and has zero relative degree. Assuming that the $P(q)$ is an exact model of the plant, it can be verified that the convergence rate is $\gamma = 0$. That is, convergence occurs in just one iteration and the converged error is $e_\infty = 0$.

One of the immediate difficulties with the plant inversion approach occurs when dealing with non minimum phase systems, in which direct inversion of the plant $P(q)$ results in an unstable filter. Although finite-duration iterations ensure bounded signals, the unstable filter undoubtedly generates undesirably large control signals. This problem can be avoided by using a stable inversion approach, which results in noncausal learning function. For nonlinear systems, direct inversion of the dynamics may be difficult. However, in some cases, inversion of the dynamics linearized around the dominant operating conditions may be sufficient to achieve good results [19].

Whether $P(q)$ is minimum phase or not, the success of the plant inversion method ultimately depends on the accuracy of the model. A mismatch between the model $P(q)$ and the actual dynamics $P(q)$ prevents convergence from occurring in one iteration. Furthermore, mismatch can lead to poor transient behavior.

To work around this problem, one can use a stable pseudo-inverse of the nominal plant. Assume that

$$\hat{P} = \frac{B_a(z)B_u(z)}{A(z)} \tag{3.9}$$

Where A and B are polynomials of z , B_u includes all uninvertible zeros. A stable pseudo-inverse of P is

$$P^{\dagger} = \frac{\mathrm{A}(z)B_u(z^{-1})}{B_a(z)[B_u(1)]^2} \tag{3.10}$$

This model has shown to have a near-unit response, i.e., it has zero phase over all frequencies and maintains a 0dB gain up to a certain frequency [18].

3.4 Problem Formulation

To this end, in order to study how these factors such as rise rate and duration have an effect on the pathophysiology of a head induced trauma. A fluid percussion injury device must be operational to perform desired pressure profiles. A linear voice coil actuator will be used with controller and identification of the system will be carried out along with an open-loop control known as ILC. This control alters the input signal until the signal converges to a signal that guarantees output of the desired signal after being passed through the controller.

3.5 Objectives

The objectives are:

1. Identify and extract a plant model from the linear drive-controller configuration from which will be utilized in the ILC algorithm.

2. Since the plant is not guaranteed to be accurate due to the limited sampling by the system, more than one ILC version will be tested. The ILC design with appropriate learning function and a proper Q-filter will be chosen to give an acceptable number of iterations for convergence.

3. Results will be compared and validated with output of controller.

CHAPTER 4

RESULTS

4.1 Creating Input Signal

MATLAB generated the desired input signal; sinusoidal waveforms were the most popular waveforms considering the direct applications. Amplitude and period were the primary parameters altered.

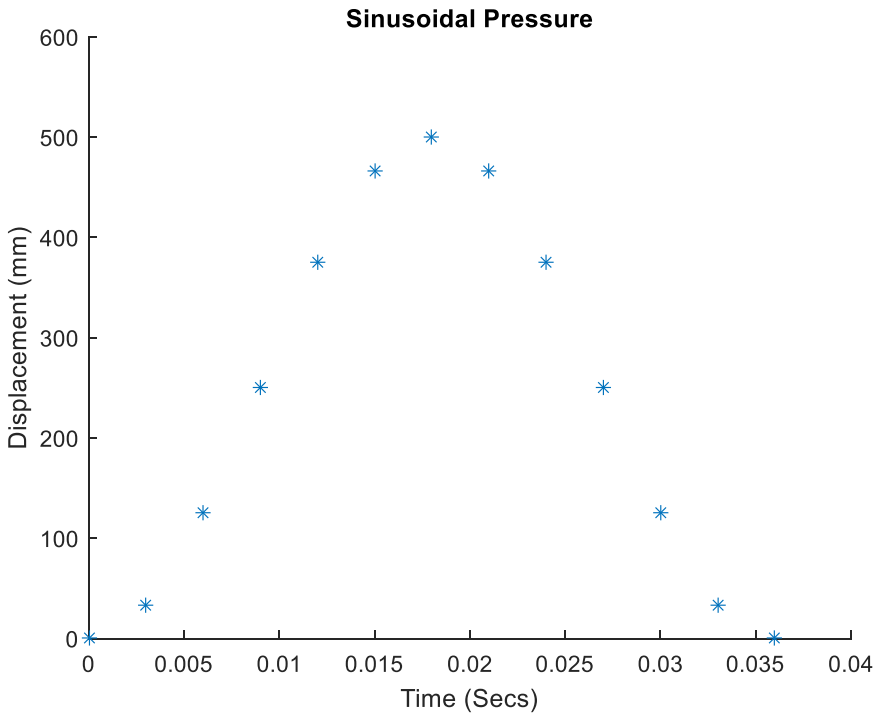

Figure 4.1 Pictured is a Sinusoidal pressure wave generated in MATLAB.

Following the creation of the desired pressure wave. The data points comprising the signal were then placed into an excel sheet which generated the following velocity segments in the following sub section to feed into the QCI Silver Sterling S3-IG controller as a text file.

4.1.1 Interpolated Motion Segment

The QCI Silver Sterling controller generates a trajectory for the linear drive to follow via an interpolated motion segments (IMS). It does this through a series of velocity segment motion commands. Below is the input signal from the previous figure prepared for the controller to feed to the linear drive as motion commands. It is clear the sinusoidal nature extends from the cyclic nature of the position plot.

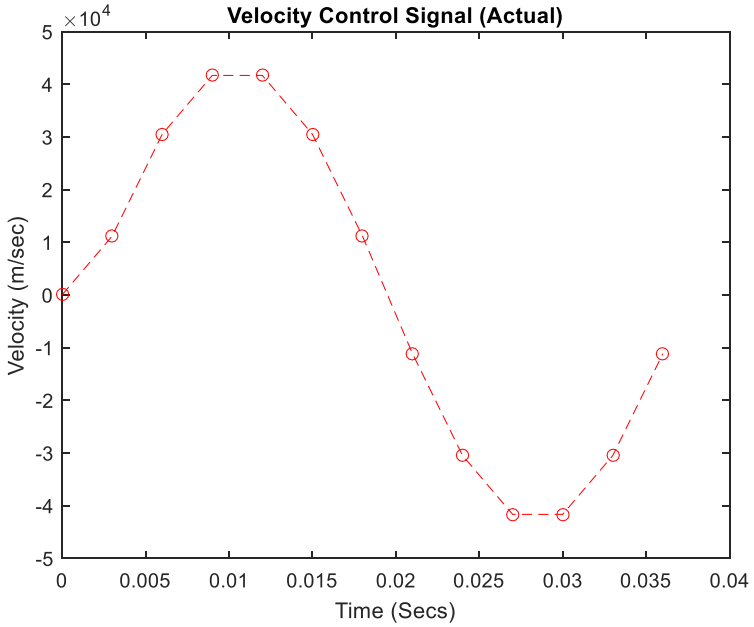

Figure 4.2 Velocity segments are ready to be sent to linear drive for operation for Sinusoidal pressure wave.

The controller generates the segments by calculating required velocity and acceleration to reach consecutive positions.

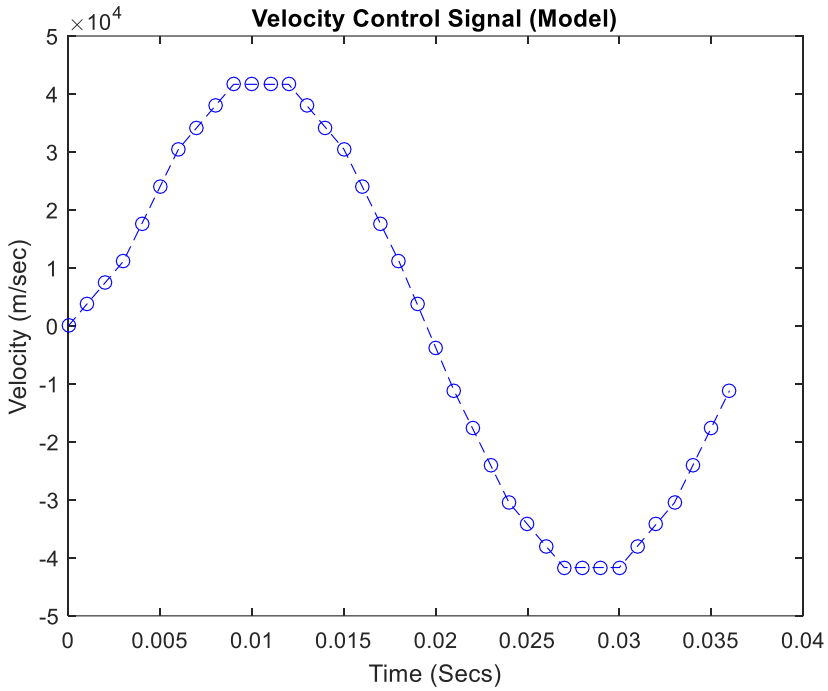

Figure 4.3 Interpolated control signal used to model and extract transfer function picture above. Values are approximated from constant acceleration over every 3-milliseconds.

It was discovered that the default settings of the controller produces a new motion command every 3-milliseconds. Hence, the control signal was adjusted such that sequential intervals of 3-milliseconds contained a velocity segment with constant acceleration as pictured in Figure 4.3

4.2 Plant Identification

Least Squares was utilized in finding the transfer function of the plant. The following equation for least squares regression is as follows:

$$y = \sum_{m=0}^{M} w_m{}^T x^m + z \tag{4.1}$$

Where y is the target or output signal, x is the input, w is the coefficients of x and z is noise usually Guassian. The regression was performed on a discrete transfer function of the form:

$$H(z) = \frac{a_o + a_1 z^{-1} + a_2 z^{-2} + \ldots + a_n z^{-n}}{1 + b_1 z^{-1} + b_2 z^{-2} + \ldots + b_n z^{-n}} \tag{4.2}$$

Multiple regressions were attempted for first, second, third and fourth order regressions. These results were also cross validated with a transfer function estimator in MATLAB that included a nonlinear estimator called “tfest”. It was found that a second order discrete transfer function was the optimal fit. Table 4.1 shows some the transfer functions that were attempted along with their averaged RMS percent difference from data:

Table 4.1 Transfer Function Results

Transfer Function	**Percent Fit to Data**
$\frac{0.2015 - 0.01989\,z^{-1}}{1 - 1.007z^{-1} + 0.01474z^{-2}}$	64.01%
$\frac{0.2018 - 0.02854\,z^{-1} + 0.008503z^{-2}}{1 - 1.421z^{-1} + 0.4169z^{-2} + 0.007759z^{-3}}$	64.02%
$\frac{0.2078 - 0.02562\,z^{-1} - 0.01094z^{-2} + 0.01583z^{-3}}{1 - 1.247z^{-1} - 0.5017z^{-2} + 0.7476z^{-3} + 0.002446z^{-4}}$	65.52%

Least squares was performed on a separate data set from the set “tfest” was implemented upon, after which the coefficients were cross-validated with the predicted transfer functions. Normalize root mean square error is pictured in the second column of Table 4.. A second order infinite impulse response model with two poles and one zero offered the most consistent simulations results when compared to actual controller response.

4.3 Iterative Learning Control Design

Simulations were conducted in Simulink implementing two different ILC schemes, which is PD tuning ILC and Plant Inversion ILC. Figure 4.1 shows the Simulink model of the PD ILC.

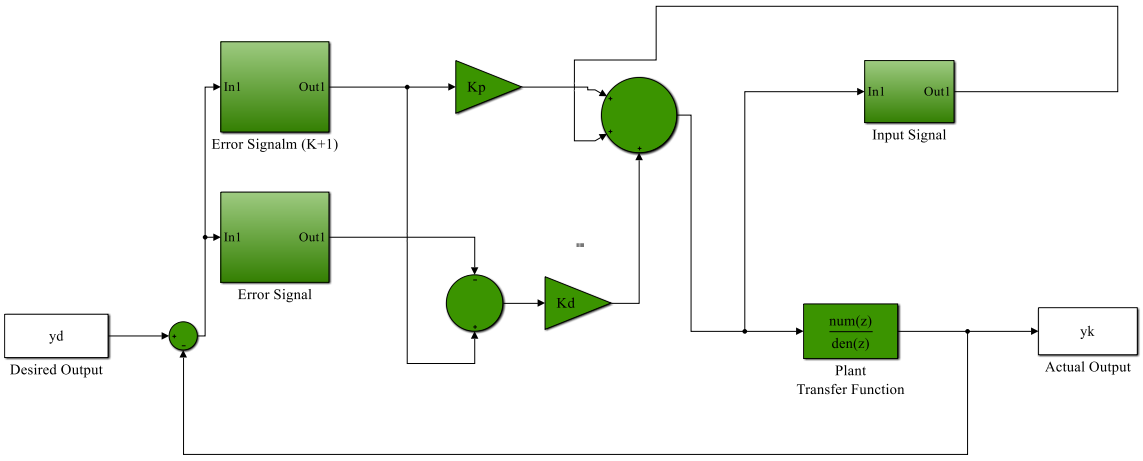

Figure 4.4 A system block diagram of PD ILC

PD ILC converged to a sinusoidal input in approximately 3 iterations for pressure waves. The selection of the gains from trial and error did not appear to change the number of iterations drastically. The error converges after 3 iterations to a local minimum value using K_p and K_d values of 36 and 9 respectively.

The next model attempted was the Inversion plant ILC. The Simulink model is shown in Figure 4.5.

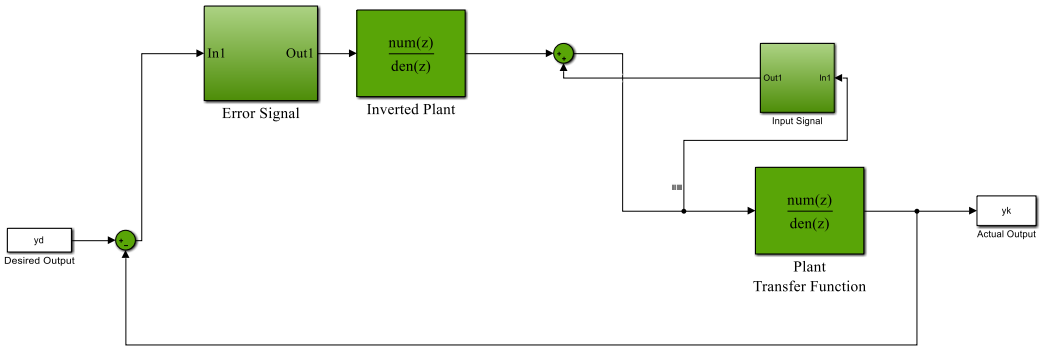

Figure 4.5 Plant inversion Simulink model with inverted plant in place of gains. The model converges in one iteration to desired signal.

After attaining the new input signal u(k) from the converged results of the Simulink model, these new signals were passed through the FPI controller in the laboratory and their resulting pressure waves recorded. The pressure waves collected were plotted against the desired output signal as show in the Results section to confirm the accuracy of the two models.

4.4 Pressure Wave Statistics

The ILC scheme with the better results was assessed with pressure wave characteristics including peak pressure, rise rate and impulse, in this PD ILC. Rise rate was calculated as the pressure increase from 10% to 90% of peak pressure. Impulse of the pressure waveform is a representation of the total energy transferred to the brain tissue and was calculated as the area under the pressure wave recording using the formula:

$$I = \sum_{t=s}^{e} P(t) \tag{4.3}$$

Where I is the impulse (units PSI-s), $P(t)$ is the pressure waveform, $t = s$ is the start of the positive pressure region, $t = e$ is the end of the positive pressure region.

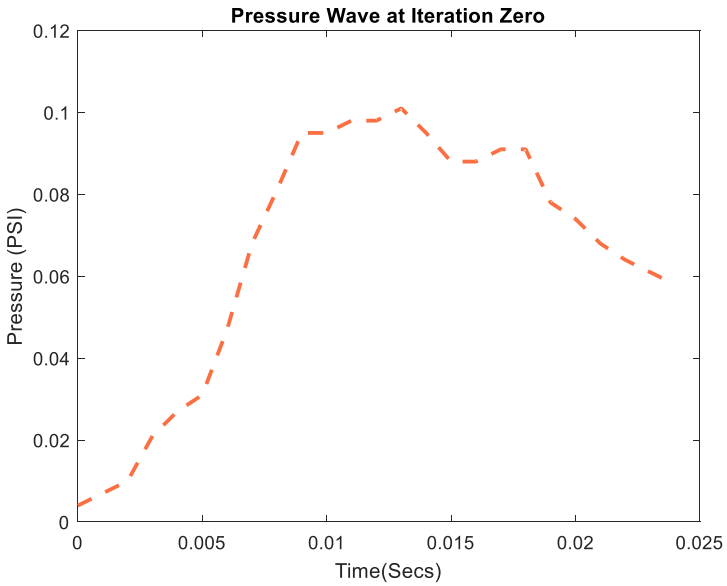

Figure 4.6 Controller response for sinusoidal pressure wave of 5 PSI Peak Pressure and 24ms duration at zeroth iteration of PD ILC.

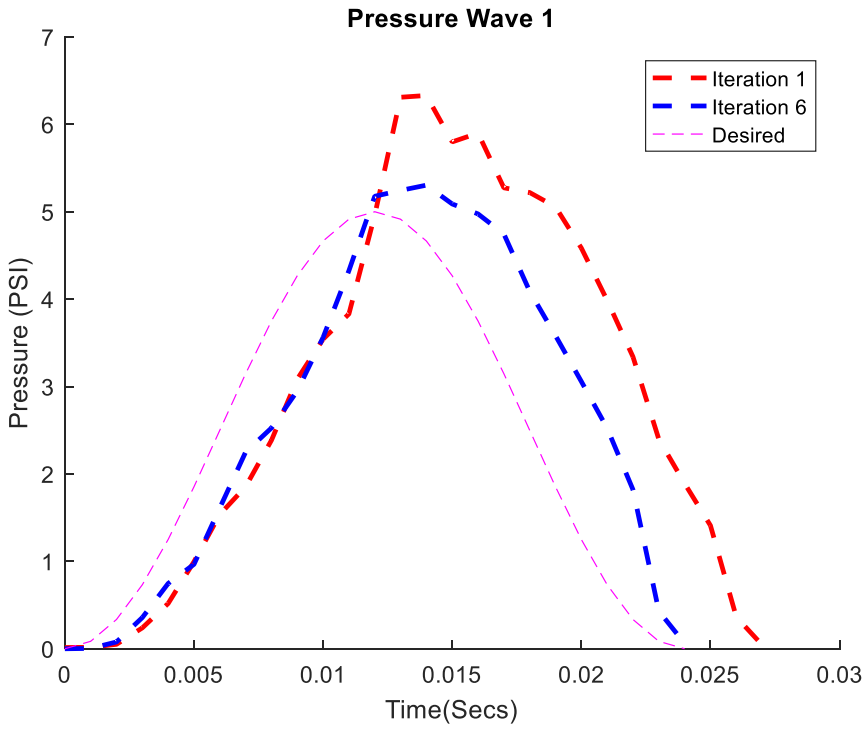

Figure 4.7 First and Second iteration response from controller for desired Sinusoidal Pressure wave of 5 Peak Pressure and 24-millisecond duration in magenta.

All measurements had a standard error of $\pm$ 1ms along with pressure error of $\pm$ 0.0005 PSI. Error in Table 4.2 and consecutive tables was calculated taking the difference between the sixth iteration value and the desired value and expressing it as a percentage of the desired value.

Table 4.2 Pressure Wave Characteristics for PD ILC

Iteration Number	Peak Pressure (PSI)	% Error (5 PSI Desired)	Rise Time (ms)	% Error (10 ms Desired)	Impulse (PSI-s)	% Error (0.06 PSI-s Desired)
0	0.101	97.98%	7.0	30%	0.0016	97.33%
1	6.33	26.60%	9.0	10%	0.0809	34.83%
3	5.304	6.08%	9.0	10%	0.0654	9.00%
6	5.305	5.08%	9.0	10%	0.0654	9.00%

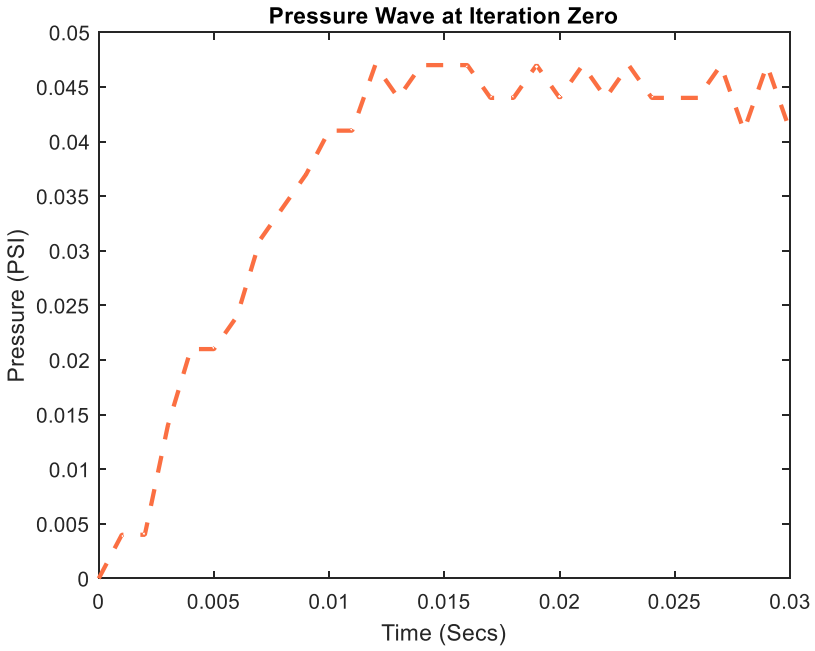

Figure 4.8 Controller response for sinusoidal pressure wave of 2 PSI Peak Pressure and 30-millisecond duration at zeroth iteration of PD ILC.

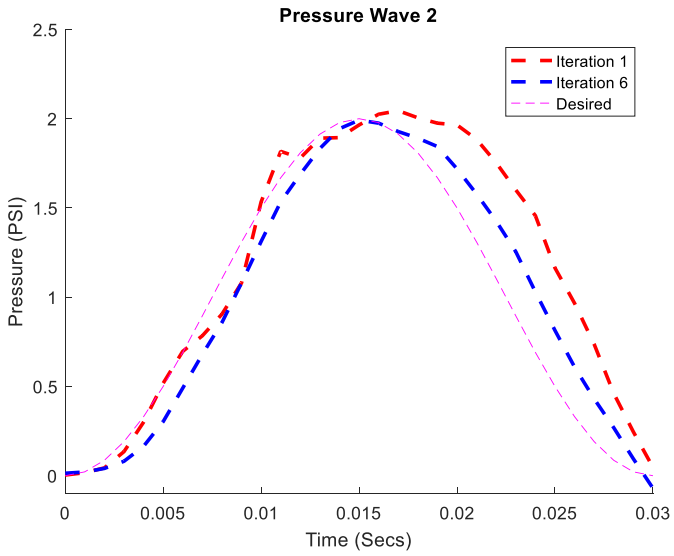

Figure 4.9 First and Second iteration response from controller for desired Sinusoidal Pressure wave of 2 PSI Peak Pressure and 30-millisecond duration in magenta.

Table 4.3 Pressure Wave Characteristics for PD ILC

Iteration Number	Peak Pressure (PSI)	% Error (2 PSI Desired)	Rise Time (ms)	% Error (9 ms Desired)	Impulse (PSI-s)	% Error (0.03 PSI-S Desired)
0	0.047	97.65%	10.0	11.11%	0.0140	66.34%
1	2.045	2.25%	10.0	11.11%	0.0357	19.00%
3	1.992	0.4%	13.0	44.44%	0.0309	3.00%
6	1.997	0.15%	13.0	44.44%	0.0309	3.00%

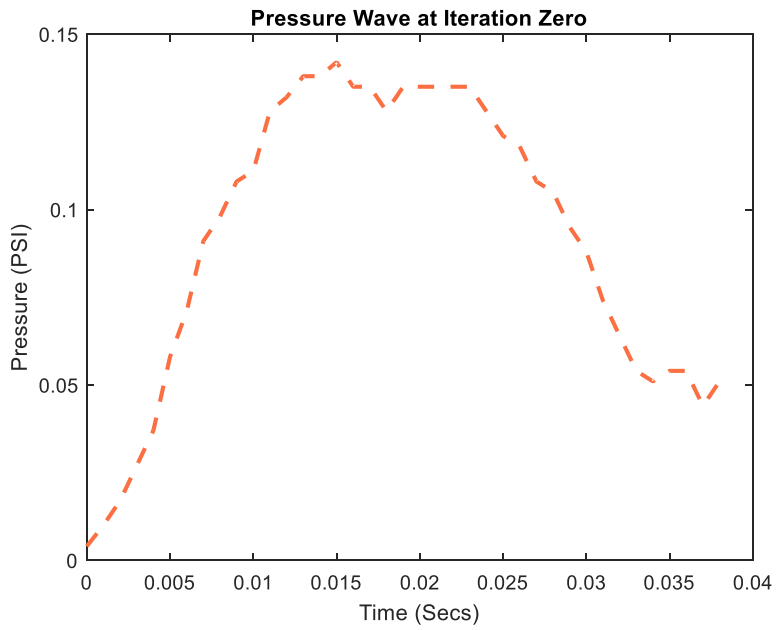

Figure 4.10 Controller response for sinusoidal pressure wave of 5 PSI Peak Pressure and 36-millisecond duration at zeroth iteration of PD ILC.

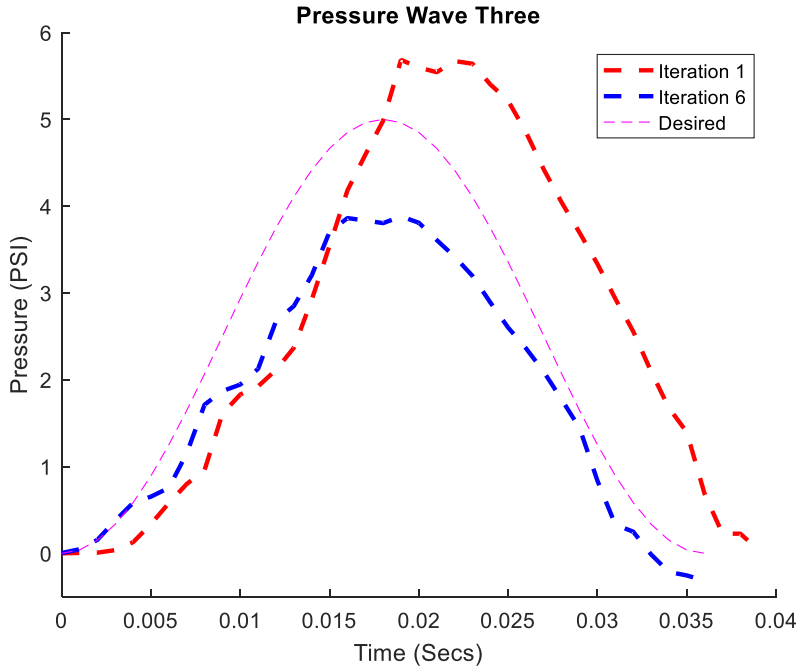

Figure 4.11 First and second iteration response from controller for desired Sinusoidal Pressure wave of 5 Peak Pressure and 36-millisecond duration in magenta.

Table 4.4 Pressure Wave Characteristics for PD ILC

Iteration Number	Peak Pressure (PSI)	% Error (5 PSI Desired)	Rise Time (ms)	% Error (12 ms Desired)	Impulse (PSI-s)	% Error (0.03 PSI-S Desired)
0	0.142	97.16%	10.0	16.67%	0.0014	95.33%
1	5.685	13.70%	14.0	16.67%	0.0357	19.00%
3	3.882	22.36%	12.0	< 8.00%*	0.0309	0.03%
6	3.893	22.14%	12.0	< 8.00%*	0.0308	2.67%

* Due to sampling resolution of 1 millisecond, we can be certain error is at most 8%

Impulse was calculated using the "trapz" function in MATLAB. Impulse for the iterations had average values of 0.2788, 0.2476 Pa-s for Figures 4.2 to 4.3 respectively. It should be noted that rise time had a resolution of 1-millisecond. PSI measurements were sub 10 PSI and the plant generated was only tested in this regime. The controller itself had PID settings of K_p = 12, K_i = 0, and K_d = 0 whilst performing experiments and following motion commands. Finally, after the sixth iteration all pressure waves maintained the same shape and impulse, rise time, and peak pressure values were within 0.01% error of the desired values.

CHAPTER 5

CONCLUSIONS

Plant estimation for this model was not approximate and two different methods were utilized and compared against each other. The inversion ILC scheme did not perform well and thus PD ILC was further investigated as the primary tool of choice. As inverting a plant is not robust against system variation and uncertainty, it was expected PD tuning ILC would fare better in practice as the final data did indeed show and is apparent from Figure 5.1.

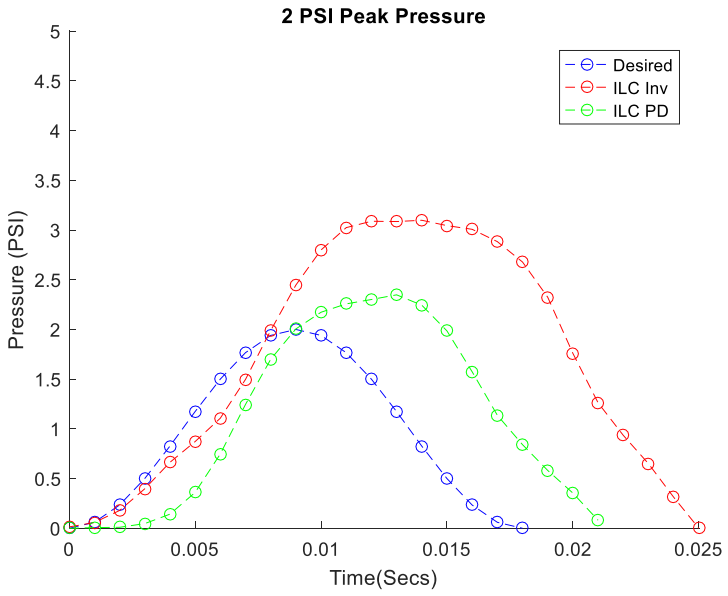

Figure 5.1 Blue, red, and green curves are for the desired, ILC Plant Inversion, and ILC PD tuning signal.

Additionally, whilst collecting data for plant identification, it was noted that most pressure waves recorded and collected for regressing the transfer function were not fast

(<20-milliseconds) and hence gives reason to believe that the present plant model is not accurate for generating percussion injury waves that are faster than 24-milliseconds. The controller is capable of producing pressure waves with semi-accurate tracking for durations of greater than 24-milliseconds from the tabulated error. If larger amplitude pressure profiles exceeding 10 PSI were desirable, then the K_p gain of the controller would have to be increased and another plant to be regressed.

REFERENCES

[1] Hyder AA, Wunderlich CA, Puvanachandra P, Gururaj G, Kobusingye OC. The impact of traumatic brain injuries: a global perspective. NeuroRehabilitation2007;22(5):341–53.

[2] Cater HL, Sundstrom LE, Morrison B 3rd. Temporal development of hippocampal cell death is dependent on tissue strain but not strain rate. J Biomech 2005.

[3] Magou GC, Guo Y, Choudhury M, Chen L, Hususan N, Masotti S, et al. Engineering a high throughput axon injury system. J Neurotrauma 2011;28(11):2203–18.

[4] Ganpule S, Alai A, Plougonven E, Chandra N. Mechanics of blast loading on the head models in the study of traumatic brain injury using experimental and computational approaches. Biomech Model Mechanobiol 2013;12(3):511–31.

[5] Sundaramurthy A, Alai A, Ganpule S, Holmberg A, Plougonven E, ChandraN. Blast-induced biomechanical loading of the rat: an experimental and anatomically accurate computational blast injury model. J Neurotrauma2012;29(13):2352–64.

[6] Faul F, Xu L, Wald MM, Coronado VG. Traumatic brain injury in the United states: emergency department visits, hospitalizations and death 2002-2006. Atlanta, GA: Centers for Disease Control and Prevention, National Center for Injury Prevention, National Center for Injury Prevention and Control; 2010.

[7] Smith DH, Meaney DF. Axonal damage in traumatic brain injury. Neuroscientist 2000

[8] Meaney DF, Smith DH Shreiber DI, Bain AC, Miller RT, Rose DT, et al. Biomechanical analysis of experimental diffuse axonal injury. J Nuerotrauma 1995.

[9] Cortez SC, McIntosh TK, Noble LJ. Experimental fluid percussion brain injury; vascular disruption and neuronal and glial alterations. Brain Res 1989

[10] Sundaramurthy A, Alai a, Ganpule S, Holmberg A, Plougonven E, Chandra N. Blast-induced biomechanical loading of the rat: an experimental and anatomically accurate computational blast injury model. J Neurotrauma 2012.

[11] Dail WG, Feeney DM, Murray HM, Linn RT, Boyeson MG. Responses to cortical injury: II. Widespread depression of the activity of an enzyme in cortex remote from a focal injury. Brain Res 1981.

[12] Dixon CE, Lyeth BG, Povlishock JT, Finding RL, Hamm RG, Marmarou A, et al. A fluid percussion model of experimental brain injury in the rat. J Neurosurg 1987.

[13] Smith DH, Chen XH, Xu BN, McIntosh TK, Gennarelli TA, Meaney DF. Characterization of diffuse axonal pathology and selective hippocampal damage following inertial brain trauma in the pig. J Neuropathol Exp Neurol 1997.

[14] Pfister BJ, Weihs, TP, Betenbaugh M, Bao G. An in vitro uniaxial stretch model for axonal injury. Ann Biomed Eng 2003.

[15] Osier, Nicole D., and Edward Dixon. "The Controlled Cortical Impact Model: Applications, Considerations for Researchers, and Future Directions." Frontiers in Neurology 7.134 (2016-August-17)

[16] R.Abdul-Wahab, B. Swietek, S. Mina, S. Sampath, V. Santhakumar and B. J. Pfister, "Precisely controllable traumatic brain injury devices for rodent models," 2011 IEEE 37th Annual Northeast Bioengineering Conference (NEBEC), Troy, NY, 2011, pp. 1-2.

[17] Bristow, D., Tharayil, M., and Allelyne, A., 2006. “A survey of iterative learning control”. Control Systems, 26(3), June, pp. 96-114.

[18] Tomizuka, M., 1987. “Zero phase error tracking algorithm for digital control”. Journal of Dynamic Systems, Measurement, and Control, 109(1), pp. 65-68.

[19] C.Wang, Z. Wang, C. Peng, Y. Zhao, and M. Tomizuka, “Compensating flexibility in servo systems using iterative learning control,” in ASME 2015 Dynamic Systems and Control Conference, pp. DSCC2015-9659, American Society of Mechanical Engineers, 2015.